Paleoceanography and Paleoclimatology

RESEARCH ARTICLE
10.1029/2018PA003510

Key Points:
- The ENSO teleconnection to North American hydroclimate varies in magnitude and spatial impact on multidecadal timescales
- The strongest and most stable ENSO influence is observed in the TexMex sector of northern Mexico and the borderlands of southwestern United States
- Tree rings reproduce these temporal and spatial changes and suggest that the changes may arise in part from North Atlantic SST variations

Supporting Information:
- Supporting Information S1

Correspondence to:
M. C. A. Torbenson,
mtorbens@uark.edu

Citation:
Torbenson, M. C. A., Stahle, D. W., Howard, I. M., Burnette, D. J., Villanueva-Díaz, J., Cook, E. R., & Griffin, D. (2019). Multidecadal modulation of the ENSO teleconnection to precipitation and tree growth over subtropical North America. *Paleoceanography and Paleoclimatology*, *34*. https://doi.org/10.1029/2018PA003510

Received 30 OCT 2018
Accepted 22 APR 2019
Accepted article online 29 APR 2019

Multidecadal Modulation of the ENSO Teleconnection to Precipitation and Tree Growth Over Subtropical North America

M. C. A. Torbenson[1], D. W. Stahle[1], I. M. Howard[1], D. J. Burnette[2], J. Villanueva-Díaz[3], E. R. Cook[4], and D. Griffin[5]

[1]Department of Geosciences, University of Arkansas, Fayetteville, AR, USA, [2]Department of Earth Sciences, University of Memphis, Memphis, TN, USA, [3]INIFAP, Gómez Palacio, Durango, Mexico, [4]Lamont-Doherty Earth Observatory, Columbia University, New York, NY, USA, [5]Department of Geography, Environment and Society, University of Minnesota, Minneapolis, MN, USA

Abstract The teleconnection of the El Niño/Southern Oscillation (ENSO) to instrumental precipitation and temperature during the cool season over North America is strongest and most temporally stable in the TexMex sector of northern Mexico and the borderlands of southwestern United States. The ENSO impact on North American hydroclimate expands and contracts out of this region on multidecadal timescales, possibly associated with the positive and negative phases of the Atlantic Multidecadal Oscillation. A subset of tree-ring chronologies from the TexMex sector also has the strongest and most stable ENSO signal detected in the North American network, similar to the strong ENSO signal measured in instrumental climate data from the same region. This subset of chronologies is used to reconstruct the multivariate ENSO index (MEI) as a measure of ENSO impact on North American hydroclimate during the instrumental and preinstrumental eras. The reconstruction exhibits improved fidelity in the frequency domain and better registration of spatial changes in ENSO signal over North America when compared to an MEI reconstruction based on all ENSO-correlated tree-ring chronologies irrespective of temporal stability of correlation. When correlated with gridded instrumental and tree-ring reconstructed Palmer drought indices across North America, the stable MEI estimate reproduces the changes in spatial impact of ENSO signal measured with instrumental data, and it reveals similar multidecadal changes in prehistory, potentially linked to the Atlantic Multidecadal Oscillation. The Great Plains drought of the 1850s and 1860s may have been an example of this Pacific-Atlantic configuration.

1. Introduction

Our understanding of long-term El Niño/Southern Oscillation (ENSO) variability, including potential decadal to multidecadal changes, is limited by relatively short meteorological and oceanographic instrumental records (Brown & Comrie, 2004; Cane et al., 1993; van Oldenborgh & Burgers, 2005). Due to the relationship between ocean-atmospheric variability and regional climate, tree-ring chronologies tuned to local climate have been used as proxies to estimate preinstrumental ENSO variability (e.g., D'Arrigo et al., 2005; Li et al., 2013; Lough & Fritts, 1990; Stahle & Cleaveland, 1993). Multiproxy reconstructions of past ENSO, utilizing several different record types, have also relied heavily on North American tree-ring data (e.g., Braganza et al., 2009; Gergis & Fowler, 2009; Stahle et al., 1998). Through these reconstructions, we have gained new information about long-term ENSO variability (D'Arrigo et al., 2005; Mann et al., 2000), and the interactions between ENSO and global and regional climate (Brönnimann et al., 2007), climate extremes (Gergis & Fowler, 2006), volcanic eruptions (Adams et al., 2003; Wahl et al., 2014; Wilson et al., 2010), and wildfire activity (Kitzberger et al., 2007; Yocom et al., 2010). However, there are disagreements within and between reconstructions (Gergis & Fowler, 2006; Wilson et al., 2010), and these differences increase the uncertainty in estimates of past ENSO variability.

The ENSO teleconnection to climate variability over subtropical North America has not been stable during the instrumental era (Cole & Cook, 1998; Enfield et al., 2001; Yu et al., 2015). It has been suggested that North Atlantic sea surface temperatures (SSTs) may modulate the strength of the ENSO teleconnection to North American hydroclimatic variability (Enfield et al., 2001), and this could be a cause of some of the disagreement among tree-ring reconstructions of ENSO. The validity of any paleoclimatic reconstruction

hinges on the assumption that the relationship between the proxy record and the target climate variable has remained stable over time (Grudd et al., 2002; Lough & Fritts, 1990). Reconstructions of teleconnection indices do not only assume a time-stable relationship between local climate and proxy but also assume a stable relationship between local climate and the teleconnection in question. Any time-dependent relationship between the mode of ocean-atmospheric variability and the remote predictors can exacerbate already existing sources of uncertainty in teleconnection reconstructions (Wilson et al., 2010).

In this paper, we investigate the robustness and temporal stability of ENSO signals in 447 tree-ring chronologies from subtropical North America with respect to the phases of the Atlantic Multidecadal Oscillation (AMO). The AMO has previously been linked to precipitation variability over the United States (Sutton & Hodson, 2005) and Atlantic hurricane activity (Caron et al., 2015). Our results indicate that some chronologies that represent an important component of previous ENSO reconstructions have a time-dependent relationship with ENSO variability in the tropical Pacific. A subset of chronologies, located in the TexMex region (per Stahle et al., 1998) of northern Mexico, and the borderlands of New Mexico and west Texas, displays a stable ENSO signal across all subperiods of analysis from 1901–1991. This stable relationship with tropical Pacific SSTs is also in agreement with the temporal and spatial correlation of ENSO with instrumental precipitation data. The subset of TexMex chronologies with a stable ENSO signal is used to estimate the waxing and waning of the ENSO teleconnection to subtropical North America on multidecadal timescales over the past 340 years.

2. Data and Methods

Gridded precipitation and temperature data (0.5° × 0.5°, CRU TS 4.021; Harris et al., 2014) for the North American continent were compared to the extended multivariate ENSO index (MEI; Wolter & Timlin, 2011) for a common period of 1902–1991, as well as three subperiods (1902–1929, 1930–1959, and 1965–1991) based on the phasing of the AMO (per Enfield et al., 2001). Comparisons for a fourth subperiod (1992–2016) were calculated using the nonextended MEI (Wolter & Timlin, 2011). Each grid point was correlated with 4-month windows of MEI spanning prior October to current May (ONDJ, NDJF, DJFM, JFMA, and FMAM) with precipitation and temperature data for the same seasonal windows.

North American tree-ring chronologies from south of 42°N, publically available at the International Tree-Ring Data Bank (Grissino-Mayer & Fritts, 1997; https://www.ncdc.noaa.gov/data-access/paleoclimatology-data/datasets/tree-ring), were screened for correlation with ENSO. A total of 447 tree-ring records, including both conifer and deciduous species, spanning at least 1871–1991 were selected for analysis. Of these 447 chronologies, 116 included earlywood width (EW), latewood width, and total ring-width (TRW) variables (Torbenson et al., 2016). The other 331 records only include TRW. Chronologies were correlated with MEI for the common period 1902–1991, as well as for the three early periods. Instrumental MEI data for 1872–1901 were withheld for verification purposes. For records that contain EW, latewood width, and TRW, only the chronology with the highest correlation with a given ENSO variable for 1902–1991 was selected for further analysis. Records that displayed a significant local correlation with MEI were also compared to the gridded CRU precipitation and temperature variables for the same periods as with the ENSO data. The CRU climate data were spatially smoothened using the Queen's case approach (Lloyd, 2010) on the nine closest grid points to the tree-ring record location.

2.1. Reconstruction of the Regional ENSO Signal

Two separate reconstructions of past ENSO influence on the study region were produced in order to estimate the impact that nonstationary ENSO response may have on reconstruction fidelity and uncertainty. All chronologies were again screened for correlation with November through February MEI for an early calibration period (1902–1959). The first reconstruction only considered chronologies that also correlate significantly ($r > 0.42$) with NDJF MEI for 1960–1991 as potential predictors. This "stable" subset of chronologies (i.e., well correlated with MEI in both periods) was submitted to a principal component analysis (PCA; Jolliffe, 2002). The resulting PC1 was entered into a simple regression model with NDJF MEI as the target predictand, using the screening period (1902–1959) as calibration and 1960–1991 for independent verification. Because of the differing start dates of the individual predictor chronologies, three PC1 regression models (reconstruction nests) were produced for periods 1869–1991, 1770–1991, and 1675–1991. This process was repeated using a late calibration (1930–1991) and early verification (1902–1929) periods, resulting in three

pairs of reconstruction nests. The early and late calibration nests were then averaged (D'Arrigo et al., 2005) for each pair. The averaged nests were spliced together, using the nest of maximum number of predictors for each time period to produce a stable reconstruction of the ENSO signal in North American tree-ring chronologies from 1675–1991 (referred to as the stable reconstruction).

The same reconstruction procedure was performed on the full network of chronologies, irrespective of their multidecadal variations in correlation with the NDJF MEI during the verification period (referred to as the ALL reconstruction), and includes chronologies with both stable and nonstable ENSO signals. The two reconstructions (stable and ALL) were quantitatively and qualitatively compared to the instrumental MEI data, including spectral coherence analysis (Percival & Constantine, 2006) and sign tests (Cook & Kairiukstis, 1990). Comparisons were also made with various other previous ENSO reconstructions (e.g., D'Arrigo et al., 2005) and early documentary records of suspected El Niño and La Niña events (Gergis & Fowler, 2006). Finally, the temporal instability of ENSO influence on North American hydroclimate prior to the observational period was examined through comparing the stable reconstruction with the North American Drought Atlas (NADA; Cook et al., 1999), a gridded reconstruction of the Palmer Drought Severity Index (PDSI; Palmer, 1965; Cook et al., 2010).

3. Results

The NDJF MEI is positively correlated with instrumental winter (NDJF) precipitation across suptropical North America for the full period of analysis (1902–1991), with the highest correlations in Florida, western Cuba, and northern Mexico (Figure 1a; Allan et al., 1996). Winter precipitation is negatively correlated with MEI over western Canada and the Pacific Northwest. The MEI is also negatively correlated with instrumental winter mean temperature over subtropical North America and positively over most of Canada and Alaska (Figure 1b). The negative ENSO correlations with temperature and positive correlations with precipitation during the cool season are most strongly expressed in northern Mexico, extreme southern Texas, and New Mexico (Figure 1a,b). The ENSO teleconnections to cool season precipitation and temperature also have a strong influence on the hydroclimate response of moisture sensitive tree-ring chronologies, especially over the TexMex sector (Figure 2). Because the growth of most TexMex tree-ring chronologies is highly correlated with soil moisture delivered during the cool season (Stahle & Cleaveland, 1993), many chronologies are also well correlated with the NDJF MEI.

3.1. Stability of the ENSO Teleconnection to Climate and Tree Growth

Cool season precipitation and temperature in northern Mexico and the southwestern United States are significantly correlated with ENSO during both positive and negative phases of the AMO during the instrumental era. But the spatial pattern and intensity of the ENSO teleconnection expand and contract from this TexMex sector on multidecadal timescales (Figure 3). California precipitation was positively correlated with the MEI since 1965 (1965–1991 and 1992–2016; Figures 3c and 3d), but not during the first half of the 20th century (1902–1929 and 1930–1959; Figures 3a and 3b). The winter precipitation correlation with ENSO also weakens over Arizona, east Texas, Louisiana, and elsewhere during at least one multidecadal episode of the instrumental era (Figure 3). The ENSO teleconnection to winter temperature is most intense and widespread during negative phases of the AMO over subtropical North America (Figures 3e and 3g); however, the ENSO signal in both precipitation and temperature in the core area of the TexMex sector remains statistically significant during all four multidecadal windows of the instrumental period (Figure 3).

This stable and significant ENSO teleconnection to instrumental precipitation and temperature is also stable and significant in a subset of North American tree-ring chronologies located in the TexMex sector. The ENSO correlation with the chronologies is illustrated in Figure 4 for the three multidecadal phases of the AMO (1901–1929, 1930–1959, and 1965–1991; as specified by Enfield et al., 2001). In all subperiods, the chronologies that are significantly correlated with the MEI are located primarily in northern Mexico and the southwestern United States (Figures 2 and 4a–4c). However, like the instrumental climate data, the ENSO correlation to tree growth is modulated on multidecadal timescales over California, Arizona, and east Texas. When only those tree-ring chronologies that are significantly ($r > 0.42$) correlated with the MEI during all three subperiods are mapped along with the magnitude of their correlation for their full period (1901–1991), they are all located in northern Mexico and the borderland of New Mexico

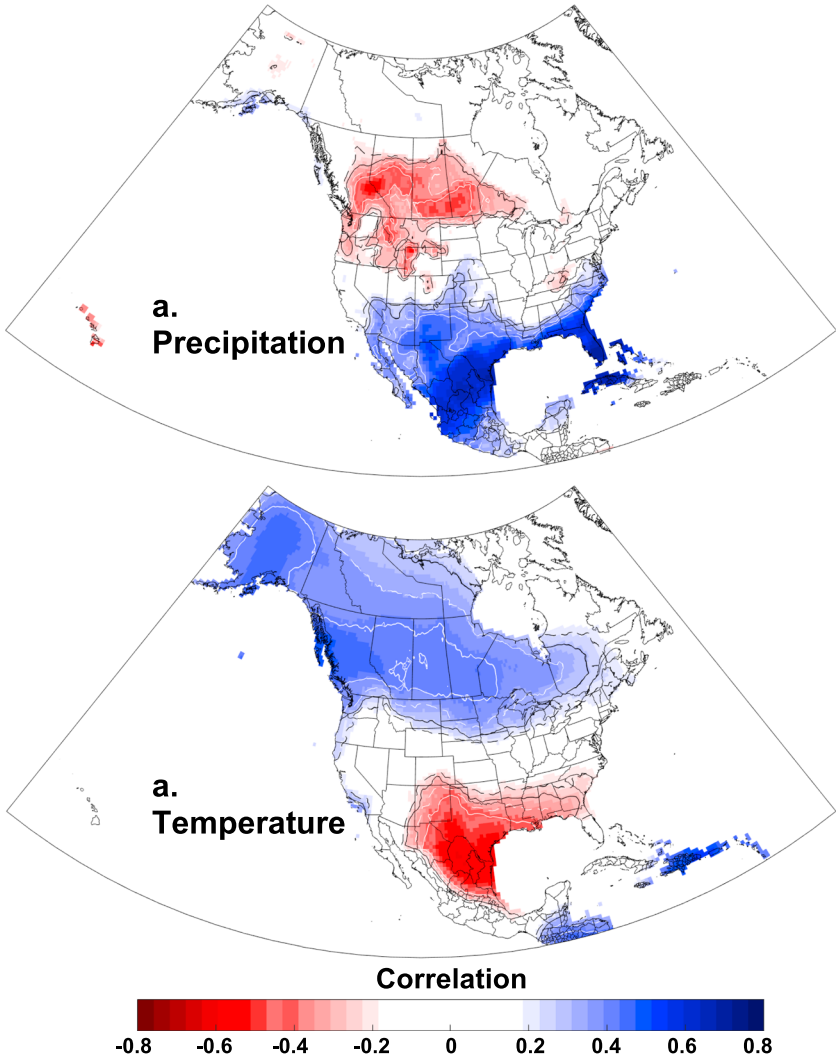

Figure 1. Correlations between instrumental NDJF extended multivariate El Niño/Southern Oscillation index and instrumental NDJF (a) precipitation and (b) temperature for the period 1901-1991. Local statistical significance contours: black dashed $p < 0.05$; black solid $p < 0.01$; white dashed $p < 0.001$; white solid $p < 0.0001$.

and west Texas (Figure 2). These TexMex chronologies have one of the strongest (Stahle et al., 1998, 2016) and most stable ENSO signals yet detected in tree-ring data worldwide, and they are located largely within the region of subtropical North America with the strongest and most stable hydroclimate response to ENSO (Figures 1 and 3).

The highest number of chronologies significantly ($r > 0.42$) correlated with NDJF MEI is recorded for the subperiod 1930–1959 ($n = 112$), while the number of significant correlations for the other two subperiods (1902–1929 [$n = 75$] and 1965–1991 [$n = 47$]) are considerably lower (Figure 5). The varying response to ENSO largely reflects the changes in ENSO influence on regional precipitation (Figure 3). For the first subperiod (1902–1929), most tree-ring chronologies from Texas are positively and significantly correlated with MEI (Figure 4a). In subsequent periods, when ENSO and instrumental precipitation correlations weaken, many of these chronologies also appear to lose their MEI signal (Figures 4b and 4c). However, the seasonal precipitation signal in these tree-ring chronologies does not change during these subperiods of the 20th century (Figure 5). Chronologies selected for the stable reconstruction are slightly more numerous than those that are stable over all three subperiods (due to the combination of two of the three subperiods for calibration), but all chronologies identified above make up predictors in the stable PCA for both early and late calibration (Table 1).

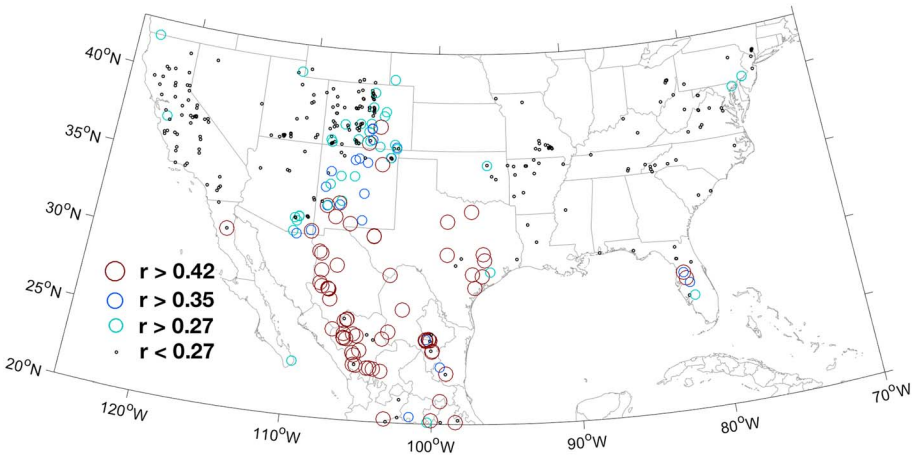

Figure 2. Magnitude of correlation between individual tree-ring chronologies and the NDJF extended multivariate El Niño/Southern Oscillation index for the period 1901-1991.

3.2. Estimating Past ENSO Influence on North American Hydroclimate With Tree Rings: Stable Versus ALL Predictors

Two sets of tree-ring chronologies were used to reconstruct the MEI. The first includes all chronologies from the North American study area that show significant correlation ($r > 0.42$) for the full period of analysis (1901–1991) with MEI (the ALL set). Between the early and late calibration periods, the combined ALL reconstruction has 104 potential predictors. The second set of tree-ring chronology predictors only includes chronologies that are significantly correlated with MEI in both the calibration and verification periods (1901–1959/1930–1991 and 1901–1929/1960–1991) and the total number of predictors in the stable set of chronologies is 27 (Table 1). The locations of chronologies used for the ALL and stable reconstructions are mapped in Figure 6.

The stable reconstruction has greater calibration and verification skill than the ALL reconstruction based on statistical evaluation of the nested reconstructions in the early, late, and combined periods of analysis (Table 2). The largest difference between the two ENSO reconstructions occurs during the early calibration period (1901–1959) when the stable reconstruction clearly outperforms the ALL version (Table 2). For the ALL predictor pool, the number of chronologies that pass screening ($r > 0.42$) for the early calibration period greatly outnumbers that of the late calibration period, in all three nest windows. Chronologies that go into the stable reconstruction make up less than 30% of the ALL chronology set for the early period and less than 40% for the late calibration period. The geographical distribution of chronologies selected for the stable reconstruction is mainly located south of the United State-Mexico border (Figure 6), especially for the late period with a well-defined region of chronologies that correlate significantly with both the calibration and verification periods (not shown).

The stable and ALL reconstructions for the MEI are compared in Figure 7. The two reconstructions are correlated at $r = 0.871$ for 1675–1991, but this correlation varies significantly over time. Regression residuals and the running correlation between stable and ALL are plotted in Figures 7c and 7d and illustrate these differences, most notably during the mid-19th century. For the period 1675–1750, there is little to distinguish the two approaches ($r = 0.926$). In later periods, for which there are a larger set of chronologies used in the PCA for the stable reconstruction, there are periods for which the two reconstructions share less than 50% of their variance (Figure 7d). The residual time series (from regressing the stable reconstruction on the ALL reconstruction; Figure 7c) displays large departures from the mean in the 1850s and 1860s, as well as in the 1900s and 1910s.

Spectral coherence analysis indicates that both reconstructions capture high-frequency MEI variability during the 20th century (Figures 7e and 7f). However, the stable reconstruction is more coherent across the entire frequency domain, especially at lower frequencies (>10 years) where the ALL lacks significant coherence with the instrumental MEI data. This difference in the spectral fidelity of the stable reconstruction of

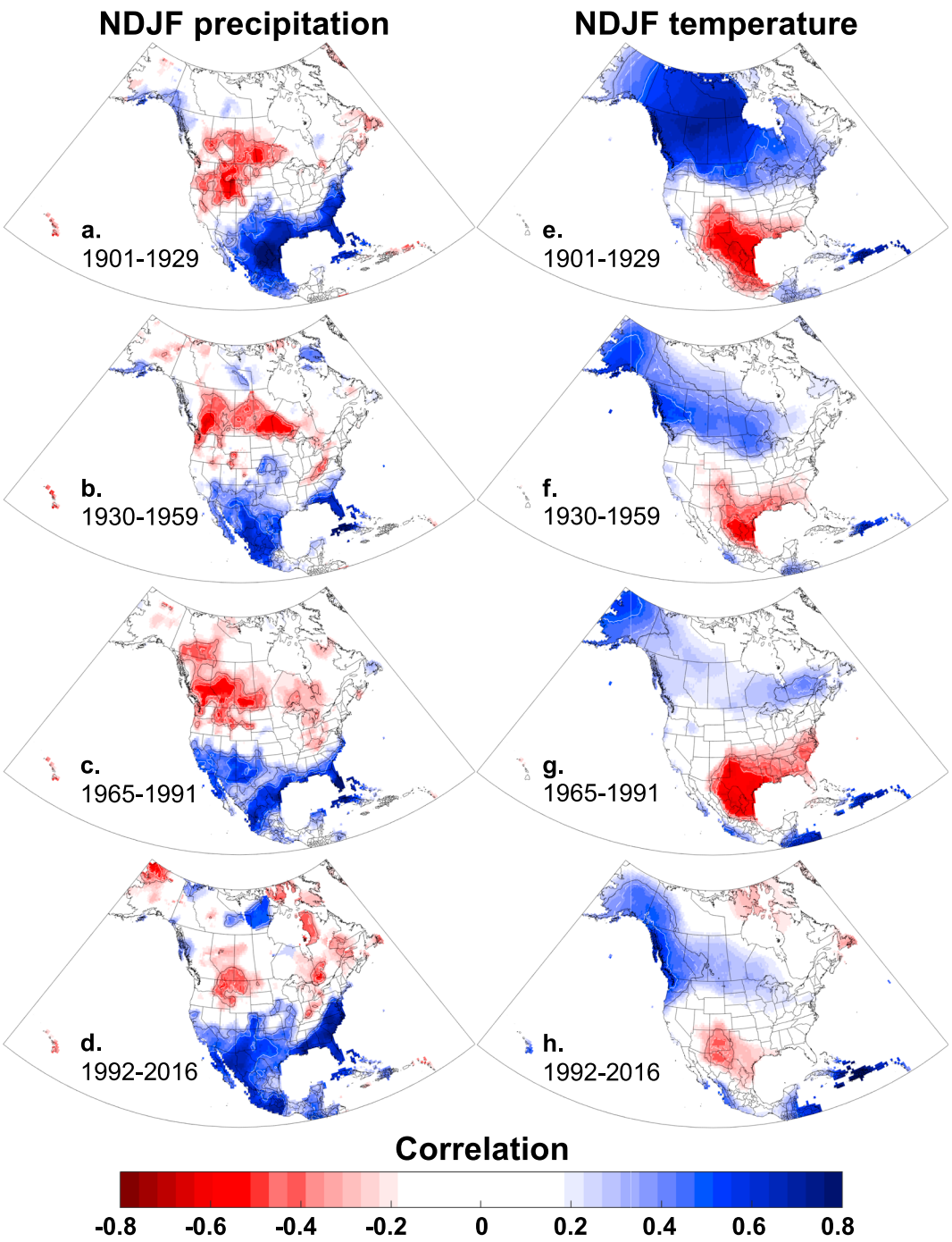

Figure 3. Correlations between instrumental NDJF extended multivariate El Niño/Southern Oscillation index (MEI) and instrumental NDJF precipitation and temperature for different subperiods. Correlations for 1992-2016 (**d** and **h**) are computed using MEI, not extended MEI. Local statistical significance contours: black $p < 0.10$; white dashed $p < 0.05$; white solid $p < 0.01$.

the MEI appears to have important implications for the estimation of low frequency spatial changes in moisture variability over North America potentially linked with ENSO.

Sign tests between reconstructions and instrumental data indicate that the stable reconstruction performs marginally better in values around the mean than the ALL ENSO estimates. The stable reconstruction has 27 misses over the full period of instrumental overlap (1872–1991), while ALL has 34. For the 10 most

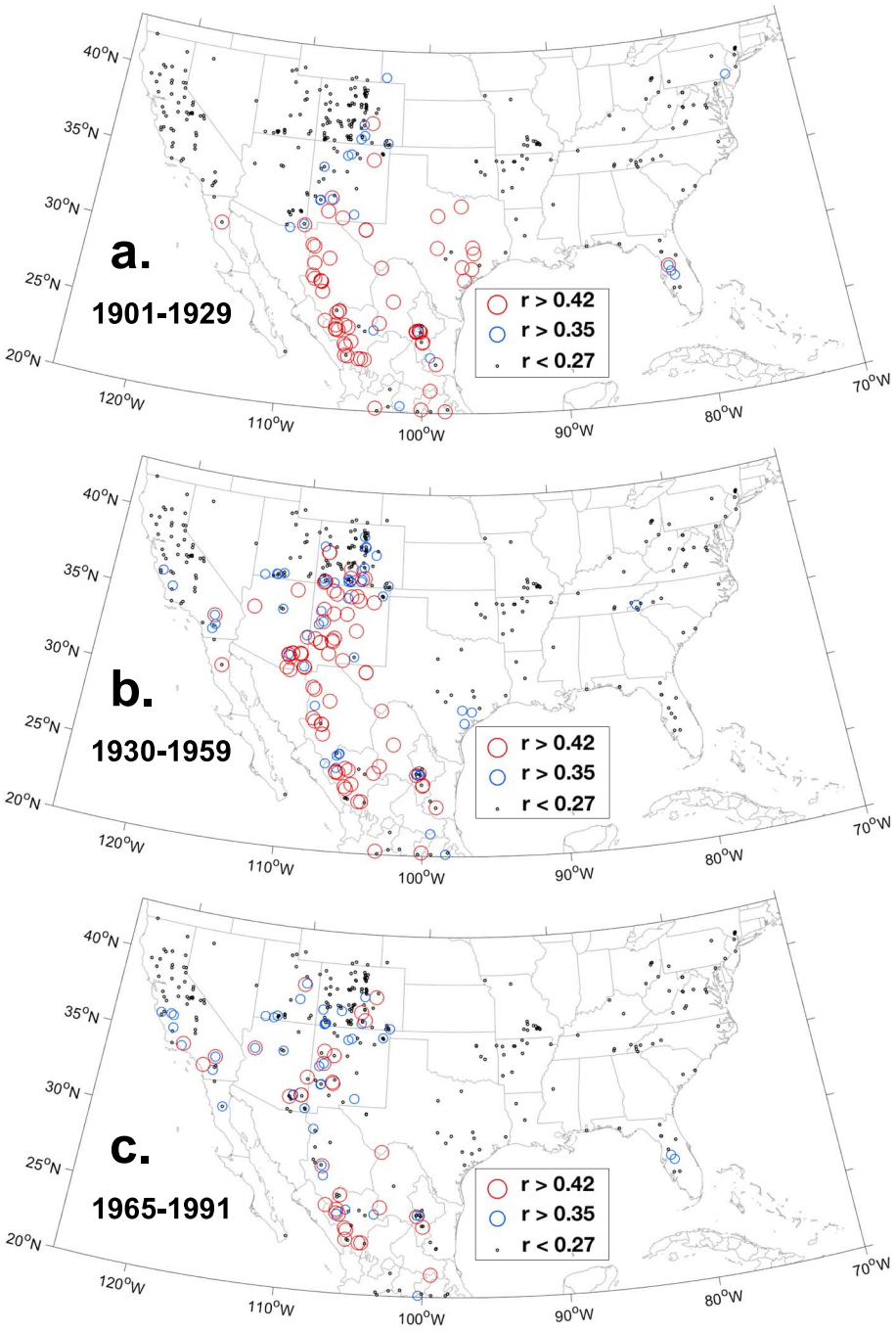

Figure 4. Same as for Figure 2 but for subperiods: (a) 1901-1929; (b) 1930-1959; and (c) 1965-1991.

extreme instrumental El Niño and La Niña events, the stable reconstruction displays the same sign for all 20 years (Table S1 in the supporting information). The ALL reconstruction has two misses, and the average difference between reconstructed and instrumental values is also higher. Overall, both reconstructions track La Niña events better than El Niño events.

4. Discussion

The influence of ENSO variability on North American precipitation and temperature during the 20th century is most prominent in the subtropical band from Baja California to Florida, where years of positive ENSO (El Niño) favor wet and cool conditions and years of negative ENSO (La Niña) favor dry and warm

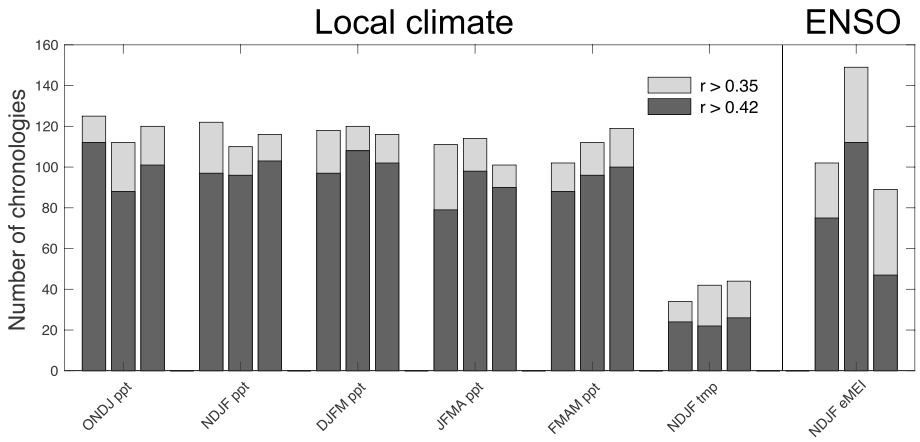

Figure 5. Barplot showing the number of chronologies from the study area that are significantly correlated with local precipitation, local temperature, and extended multivariate ENSO index for subperiods 1901-1929 (left bar), 1930-1959 (center bar), and 1965-1991 (right bar). ENSO = El Niño/Southern Oscillation.

conditions for NDJF (Figure 1). Correlations between ENSO and precipitation exceed 0.7 in northern Mexico, making the TexMex sector one of the strongest ENSO teleconnection regions on Earth (Dai & Wigley, 2000). The negative correlation between the MEI and precipitation over the Pacific Northwest is also significant (Figure 2), but it is subject to considerable multidecadal variability (Figure 3).

Because of the strong modulation of winter precipitation in the U.S. Southwest and northern Mexico by ENSO, and the dependence of regional tree growth on soil moisture recharge by winter precipitation, the

Table 1
Tree-Ring Chronologies Used as Predictors in the Stable Reconstruction of MEI

State	Site code	Site name	Species	Variable	Start date	Latitude	Longitude	Early calib.	Late calib.
CH	MDG	Guacamayas	PSME	EW	1598	30.33	-108.37		X
CH	TUT	Tutuaca	PSME	EW	1534	28.37	-108.16		X
DU	AVE	Arroyo Verde	PSME	EW	1770	25.03	-106.04	X	X
DU	CGD	Cienega Guadalupe	PIPO	EW	1675	25.04	-106.18	X	X
DU	CHU	Cerro Huehuento	PSME	EW	1552	24.05	-105.44	X	X
DU	CUE	Cueveci	PSME	EW	1770	23.30	-104.32	X	X
DU	CVS	Cuevacillas	PSME	EW	1747	25.09	-106.23	X	X
DU	PUE	Puentecillas	PSME	EW	1573	24.19	-105.55	X	X
DU	TAH	Tarahumara	PSME	EW	1724	25.34	-106.20	X	X
NM	FCU	Filmore Canyon	PIPO	EW	1306	32.20	-106.34		X
NM	SMT	San Mateo	PSME	EW	816	33.43	-107.27	X	X
CH	CAC	Cañon del Cobre	PSME	TRW	1770	28.01	-107.49	X	X
CH	CIA	Creel Airstrip	PSME	TRW	1739	27.42	-107.37		X
CH	MOH	Cerro Mohinara	PSME	TRW	1681	25.56	-107.01	X	X
CO	CHK	Chokecherry	PIED	TRW	1450	37.33	-105.34	X	
CO	WMC	Wet Mountains	PSME	TRW	1336	37.54	-105.09	X	
CU	COA	Coahuilón	PSME	TRW	1675	25.14	-103.55	X	X
CU	HUA	Huachichil	PICM	TRW	1552	25.12	-100.50	X	X
DU	BAR	Cerro Barajas	PSME	TRW	1651	26.24	-106.05	X	X
DU	BAY	Bayas	PSME	TRW	1845	23.27	-104.50	X	X
DU	BDG	Barrial Guadalupe	TAMU	TRW	1869	25.59	-103.14	X	X
NL	CHO	Chona	PICM	TRW	1573	24.44	-100.07	X	X
NM	LAT	Las Tablas	PIED	TRW	1520	36.32	-106.01	X	
NM	SAN	Sandia Mountain	PIFL	TRW	290	35.15	-107.30	X	
SL	VER	Rio Verde	TAMU	TRW	1724	21.41	-99.47	X	X
TA	SAB	Rio Sabinas	TAMU	TRW	1534	23.09	-99.09		X
TX	BSC	Big Bend	PSME	TRW	1473	29.15	-103.18	X	X

Note. The final two columns indicate if the chronology was used in early and/or late calibration model.

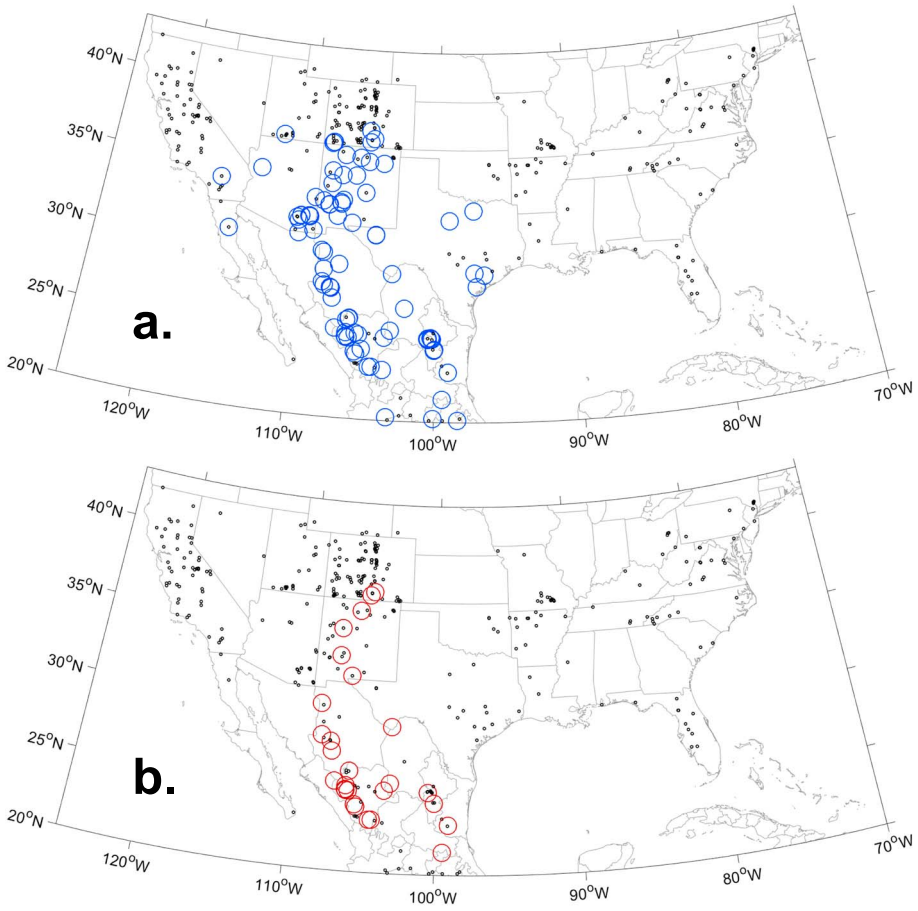

Figure 6. Locations of chronologies used for (a) the ALL (blue circles) and (b) stable (red circles) reconstructions of multivariate El Niño/Southern Oscillation index. Black dots indicate all tree-ring chronologies screened.

strongest ENSO signal in the North American tree-ring network can also be found in the TexMex sector (Figure 2; Stahle & Cleaveland, 1993). Many of the strongest correlations ($r > 0.42$) are observed with Douglas-fir (*Pseudotsuga menziesii*) EW or TRW chronologies from the Sierra Madre Occidental, including the strongest single correlation recorded by an EW chronology from Puentecillas, Durango, Mexico ($r = 0.599$; 1901–1991). With the exception of a small number of *Taxodium distichum* chronologies from Florida, few tree ring chronologies outside the North American southwest have a strong and stable correlation with ENSO indices.

The time-dependent ENSO signal in instrumental hydroclimate data for North America previously described by Cole and Cook (1998) and Enfield et al. (2001) is also present in the CRU NDJF precipitation data. The highest number of significant correlations between tree-ring chronologies and NDJF ENSO is recorded for the positive phase of the AMO (1930–1959), a period when ENSO and precipitation are also widely and significantly correlated across the TexMex sector and into Arizona, southern California, and Nevada. Many of these chronologies display lower or nonsignificant correlations for subperiods of negative AMO phasing. Only 18 of the 442 tree-ring chronologies analyzed record significant correlations with NDJF MEI for the full period of analysis and with all three subperiods. Again, the majority of these chronologies are located in the TexMex sector, and 13 are based on ring-width variables from Douglas-fir. There are few differences in the number of chronologies that are significantly correlated with *local* precipitation or temperature over the three subperiods (Figure 5). Some of the chronologies that lose significance in the earliest subperiod (1901–1929) are located in Mexico where instrumental climate data for the early 20th century are problematic (Douglas, 2007; Jauregui, 1979). Overall, there is nothing to suggest that trees in the U.S. Southwest or Mexico have changed their response to local hydroclimate variability over the 20th century.

Table 2
Common Calibration and Verification Statistics for the Stable and ALL Reconstructions

Early calibration (1901-1959), verification 1960-1991						
	r2	Ver. r	Ver. RE	Ver. CE	n	
Nest 1 stable	0.546	0.709	0.467	0.457	22	
Nest 2 stable	0.508	0.698	0.444	0.434	20	
Nest 3 stable	0.429	0.653	0.367	0.356	13	
Nest 1 ALL	0.533	0.493	0.253	0.239	78	
Nest 2 ALL	0.486	0.495	0.257	0.243	66	
Nest 3 ALL	0.445	0.453	0.218	0.204	50	
Late calibration (1930-1991), verification 1901-1929						
	r2	Ver. r	Ver. RE	Ver. CE	*n*	
Nest 1 stable	0.452	0.761	0.561	0.558	23	
Nest 2 stable	0.433	0.739	0.525	0.522	21	
Nest 3 stable	0.397	0.723	0.496	0.492	13	
Nest 1 ALL	0.366	0.430	0.026	0.020	59	
Nest 2 ALL	0.350	0.419	0.017	0.011	54	
Nest 3 ALL	0.334	0.407	0.010	0.004	45	
	Early calib. (1901-1959)		Late calib. (1930-1991)		Combined	
	ALL	stable	ALL	stable	ALL	stable
1872-1900	0.588	0.633	0.430	0.625	0.525	0.638
1901-1929	0.736	0.754	0.430	0.761	0.597	0.768
1930-1959	0.759	0.737	0.719	0.748	0.752	0.750
1965-1991	0.479	0.699	0.589	0.615	0.553	0.658
1872-1991					0.598	0.706

Note. Ver. r = verification correlation; Ver. RE = verification reduction of error; Ver. CE = verification coefficient of efficiency. Lower part shows correlations of respective reconstruction with instrumental MEI data.

Therefore, the multidecadal variability in the spatial scale of the ENSO signal to tree growth is most likely due to changes of the teleconnection to hydroclimate over North America.

Comparisons between the stable and ALL reconstructions of the MEI suggest that a regional subset of the network of over 100 chronologies has the best calibration and verification statistics. The subsequent stable reconstruction from using the 27 chronologies that display significant ENSO correlations during both positive and negative AMO phases as predictors explains over 50% of the variance for the full period (1872–1991) of instrumental MEI data overlap. Although the two reconstructions are highly correlated over the full period of reconstruction ($r = 0.871$; 1675–1991), the relationship varies greatly over time. The lowest point in the running correlation between the stable and ALL reconstructions is recorded for the 1850s and 1860s, when the stable reconstruction estimates stronger La Niña conditions (the mean for 1856–1868 in stable is -0.601 but only -0.302 in ALL). Several of the differences in this period occur during years when other multiproxy reconstructions indicate strong or very strong La Niña events (Gergis & Fowler, 2009).

4.1. Preinstrumental Variability of ENSO Influence

The relationship between ENSO and precipitation variability across North America does not appear to have been stationary during the observational era (Figure 3). Comparing the stable reconstruction with the NADA reveals changing patterns prior to the instrumental record, similar to those recorded for precipitation and soil moisture during the instrumental era (Cole & Cook, 1998). The stable reconstruction reproduces the teleconnection pattern of instrumental MEI (Figure 8a) with great fidelity (Figure 8b) for the verification period 1872–1900, with positive correlations extending into the Central Plains. Although the stable ENSO reconstruction cannot be considered independent from the NADA over the TexMex region (as the predictors are highly correlated with PDSI), spatial changes in correlations are recorded beyond the search radius of the NADA (450 km; Cook et al., 1999).

The correlations between ENSO and reconstructed PDSI are not significant in eastern Texas during 1872–1900, and also weak in western Arizona. Correlation analyses for 28-year periods during the preinstrumental era also indicate change in the spatial pattern and intensity over North America (Figures 8c–8i). For

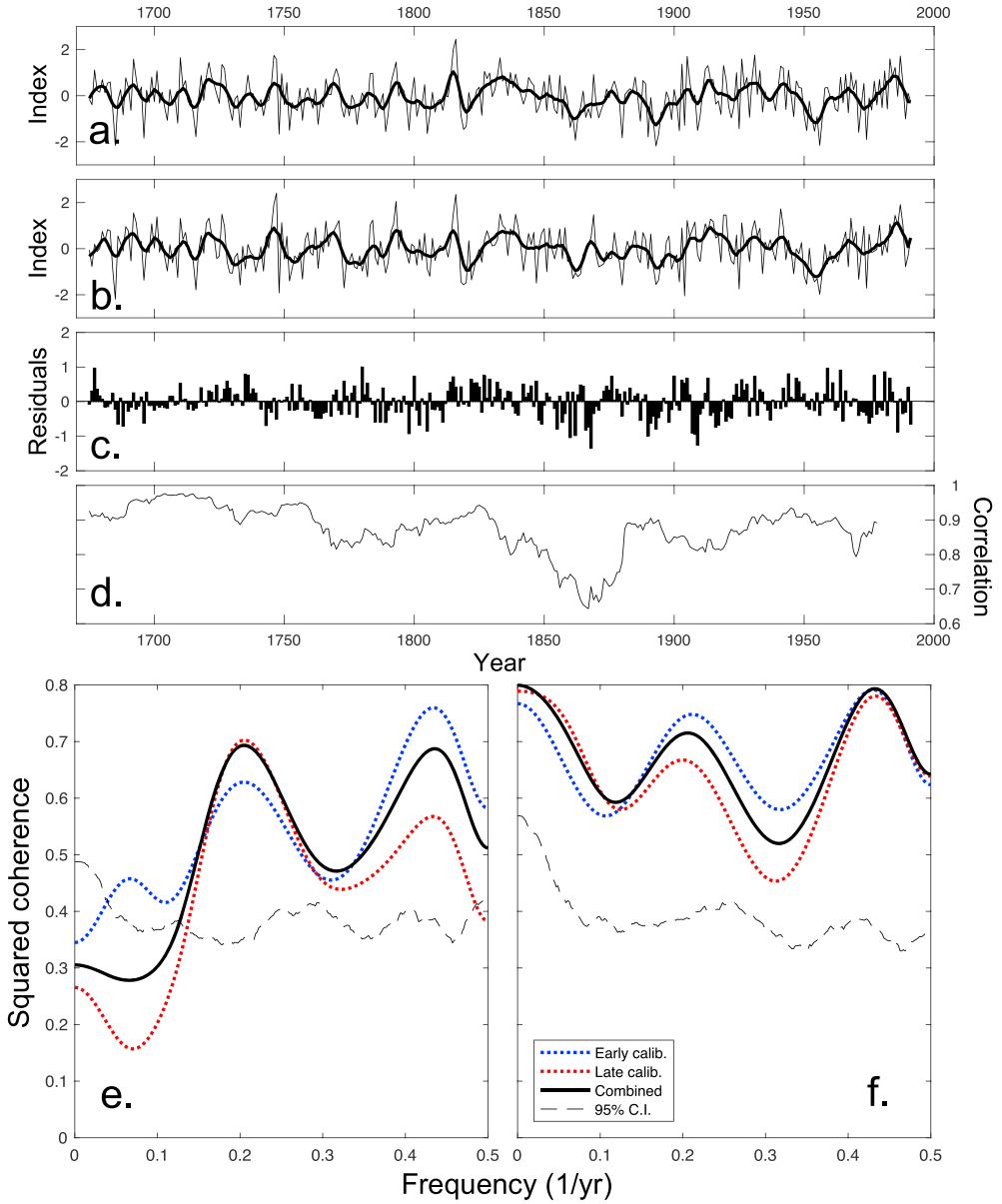

Figure 7. Reconstructions of multivariate El Niño/Southern Oscillation index from (a) ALL and (b) stable networks of tree-ring chronologies for 1675-1991. The residuals from linear regression is plotted in (c), and the running correlation (15-year window) is plotted in (d). The squared coherence between instrumental and reconstructed multivariate El Niño/Southern Oscillation index for the period 1901-1991 is plotted for (e) ALL and (f) stable.

example, the influence of ENSO on summer PDSI in eastern Texas has fluctuated between periods of strong and weak ENSO influence. The shifting magnitude of negative ENSO correlations with precipitation is also recorded during the preinstrumental era (Figure 8). There is little significant negative correlation during 1731–1758 (Figure 8g) while negative correlations are present from northern California to the Canadian border and beyond during 1843–1871 (Figure 8c) and 1787–1814 (Figure 8e).

Spatial expansion and contraction of significant ENSO correlation from the core region in northern Mexico occur on multidecadal timescales during the instrumental and preinstrumental era since at least 1675 (Figure 8). Correlations between the stable reconstruction and the NADA is significant during the 1872–1900 verification period for a large region north of the U.S. Southwest, entering South Dakota and Wyoming (Figures 8a and 8b), and similar patterns are estimated for 1815–1842 and 1843–1871

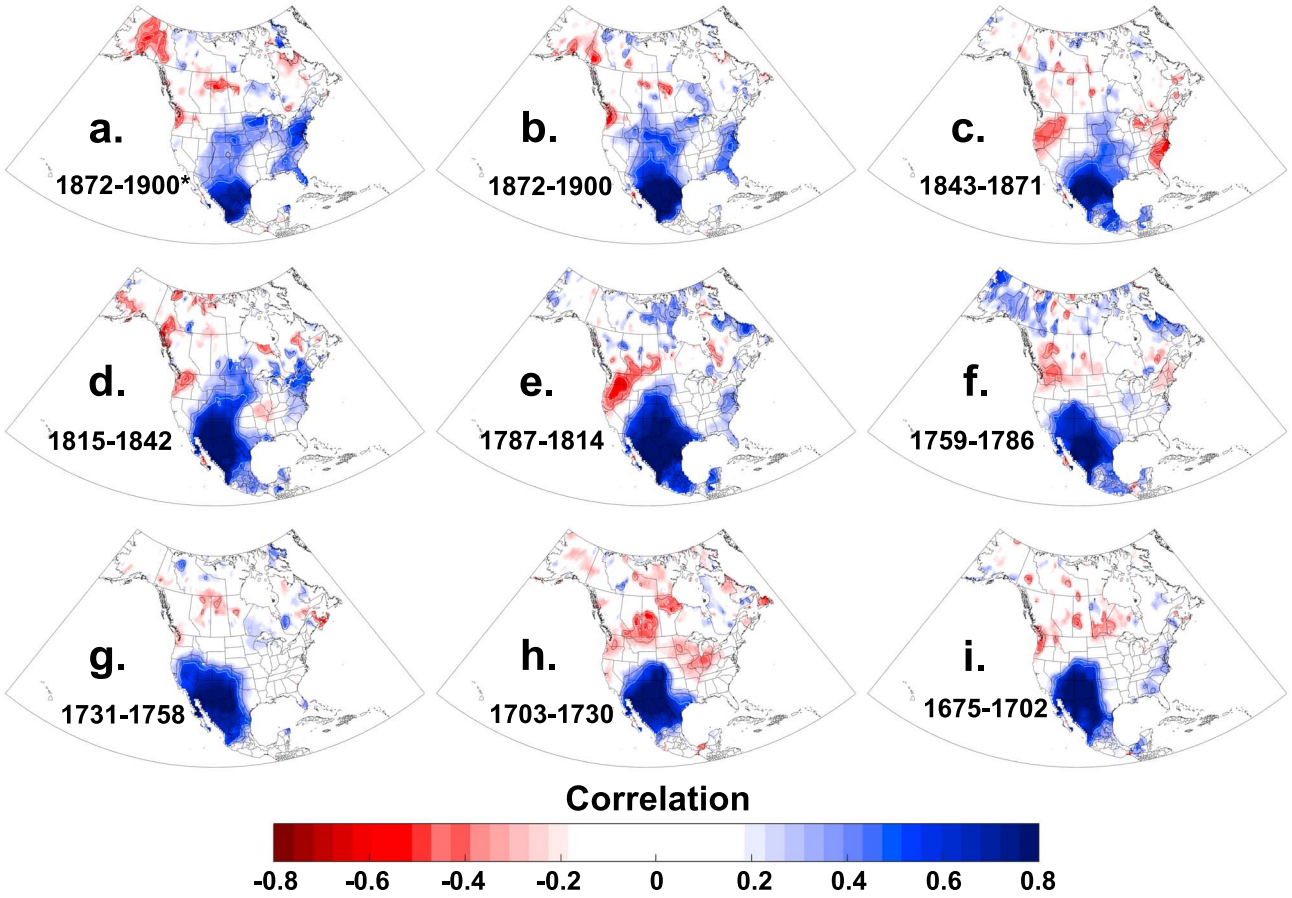

Figure 8. Correlations between (a) instrumental NDJF multivariate El Niño/Southern Oscillation index and the North American Drought Atlas and (b–h) the stable reconstruction and the North American Drought Atlas for 28-year periods. Local statistical significant contours: black $p < 0.10$; white dashed $p < 0.05$; white solid $p < 0.01$.

(Figures 8c and 8d). Expansion occurs westward during 1731–1758 (Figure 8g) during which positive correlations are recorded for all of California, analogous to the precipitation correlations recorded for the middle of the 20th century and the most recent decades (Figure 3).

4.2. The Role of Atlantic Variability on Spatial ENSO Precipitation Influence

The magnitude of correlations between ENSO and winter precipitation, and subsequent summer PDSI, has not remained static across western North America over the 20th and early 21st centuries. Possible interactions between the Pacific and Atlantic oceans have previously been suggested as drivers of drought in North America (e.g., d'Orgeville & Peltier, 2007; McCabe et al., 2004; Ruprich-Robert, 2018). Yu et al. (2015) proposed that the positive phase of the AMO is associated with an intensification of the subtropical high. Winter-to-spring atmospheric pressure conditions are more consistent across the southwest and the Great Plains during years of positive AMO and could explain why the influence of ENSO on precipitation spreads northeastward from the core TexMex region. No similar pattern is recorded for the Pacific Decadal Oscillation (Mantua et al., 1997); instead, increased differences in pressure change over western United States are associated with the Pacific Decadal Oscillation (Yu et al., 2015). Similar results on the relationship between warmer North Atlantic SSTs and drought-driven wildfire activity were found by Kitzberger et al. (2007), for which synchronous fires from the southwest to South Dakota and the upper Colorado River basin were associated with the positive phase of the AMO.

The AMO reconstruction of Gray et al. (2004) records overall negative values for the 18th century. For subperiods between 1703 and 1786, the positive correlations between the stable MEI reconstruction and the NADA are confined to the core TexMex region. However, some changes are recorded over eastern Texas,

including lessened correlations during 1731–1758 (Figure 8g), a period during which the AMO reconstruction is positive, albeit weak (0.074). Reconstructed persistence between May soil moisture and JJA atmospheric moisture balance over the central United States, thought to be driven by positive AMO, reach a high point around 1750 (Torbenson & Stahle, 2018). This change in ENSO influence over Texas is analogous to the positive AMO phase of 1930–1965. Similar drops in correlation over eastern Texas are present for 1675–1702, occurring during the strong positive AMO phase estimated for the end of the 17th century (Gray et al., 2004).

One of the most severe decadal droughts of the past 500 years in the Central Plains occurred during the 1850s and 1860s (Stahle & Cleaveland, 1988; Woodhouse & Overpeck, 1998), termed the "Civil War drought" (Herweijer et al., 2006; Stahle et al., 2011). The differences in estimated MEI between the stable and ALL reconstructions (Figure 7c) suggest stronger and more persistent La Niña conditions for the period based on the stable estimates. ENSO influence also appears to have expanded into the Great Plains during the Civil War drought, with positive correlations into Missouri and the confluence region of the Ohio and Mississippi rivers (Figure 8c). Reconstructed AMO (Gray et al., 2004) indicates the strongest positive AMO phase of the 19th century during this period, and this combination of Pacific and Atlantic conditions may have contributed to the severity of moisture deficits during the 1850s and 1860s. This configuration appears to have continued through the end of the 19th century, recorded by both instrumental and reconstructed MEI (Figures 8a and 8b). Although no exact Civil War drought analog exists for the instrumental period, positive correlations between ENSO and precipitation during the positive AMO phase of 1930–1959 extends to South Dakota and Nebraska. The mid-19th century drought appears to have been most extreme during the cool season (Howard et al., 2019; Torbenson & Stahle, 2018) and the stable reconstruction of the MEI suggest that recurrent La Niña conditions may have played a prominent role in this episode of multidecadal dryness.

Our results suggest that the low-frequency swings in spatial influence of ENSO on North American hydroclimate recorded for the observational era also occurred in centuries past. Although there are several sources of uncertainty associated with each reconstruction used in this analysis, the results are indicative of Pacific-Atlantic teleconnections similar to those that have been reported elsewhere (e.g., Cole & Cook, 1998; Kitzberger et al., 2007; Yu et al., 2015). Because the recorded changes are multidecadal in nature and seem to conform with the sign changes of instrumental and possibly reconstructed AMO indices, these low-frequency changes in the regions of subtropical North America influenced by ENSO may be driven in part by SST variability in the North Atlantic that are associated with atmospheric pressure changes over western United States.

5. Conclusions

The spatial pattern of ENSO forcing on cool season precipitation and temperature, and the subsequent growing season soil moisture balance over North America has varied over the 20th and 21st centuries. The strongest and most stable ENSO signal apparent in the instrumental precipitation and temperature observations, and the North American tree-ring network, is located in the subtropical TexMex sector of northern Mexico and the borderlands of the U.S. Southwest.

The region is not well represented by instrumental weather observations before 1950, but moisture sensitive tree-ring chronologies from the area indicate a strong and stable correlation with ENSO indices during the late 19th and early 20th centuries when regional weather observations are most limited.

Correlations between the stable ENSO reconstruction and gridded drought for preinstrumental periods display changes in magnitude and spatial influence outside of the core ENSO region, analogous to those recorded in the 20th and early 21st century instrumental data. The nonstationarity of ENSO signal recorded for the instrumental period in Arizona, southern California, and Texas appears to have been a feature of ocean-atmospheric interactions over the past 350 years. The changes in strength and spatial scale of ENSO teleconnection to North America hydroclimate could be linked to North Atlantic SST variability. The positive phase of AMO during the middle and late 19th century coincides with strong negative MEI values. The Civil War drought of the mid-19th century may therefore be an example of interaction between persistent La Niña conditions and positive AMO resulting in prolonged cool season moisture deficits over the Great Plains. These results need to be tested in observations and simulations, but understanding the

expected extent and magnitude of ENSO influence outside of the TexMex sector may be enhanced based in part on the state of the SST field in the North Atlantic.

Acknowledgments
We thank two anonymous reviewers, the editor, and assistant editor, for constructive feedback that helped improve this manuscript. We appreciate everyone who have contributed to the ITRDB for making their data publically available. The National Science Foundation (Grant AGS-1266014) and Inter-American Institute for Global Change Research (CRN 2047) funded this study. Lamont-Doherty Earth Observatory contribution No. 8315. Both reconstructions are available through the NOAA NCDC Paleoclimatology data bank (https://www.ncdc.noaa.gov/data-access/paleoclimatology-data).

References

Adams, B. J., Mann, M. E., & Ammann, C. M. (2003). Proxy evidence for an El Niño-like response to volcanic forcing. *Nature*, *426*(6964), 274–278. https://doi.org.10.1038/nature02101

Allan, R. J., Lindesay, J., & Parker, D. (1996). *El Niño/Southern Oscillation & Climatic Variability*. Clayton, Australia: CSIRO Publishing.

Braganza, K., Gergis, J. L., Power, S. B., Risbey, J. S., & Fowler, A. M. (2009). A multiproxy index of the El Niño-Southern Oscillation, A.D. 1525-1982. *Journal of Geophysical Research*, *114*, D05106. https://doi.org/10.1029/2008JD010896

Brönnimann, S., Xoplaki, E., Casty, C., Pauling, A., & Luterbacher, J. (2007). ENSO influence on Europe during the last centuries. *Climate Dynamics*, *28*(2-3), 181–197. https://doi.org/10.1007/s00382-006-0175-z

Brown, D. P., & Comrie, A. C. (2004). A winter precipitation 'dipole' in the western United States associated with multidecadal ENSO variability. *Geophysical Research Letters*, *31*, L09203. https://doi.org/10.1029/2003GL018726

Cane, M. A., Fairbanks, R. G., & Shen, G. T. (1993). Recent variability in the Southern Oscillation: Isotopic results from a Tarawa atoll coral. *Science*, *260*(5115), 1790–1793. https://doi.org/10.1126/science.260.5115.1790

Caron, L.-P., Boudreault, M., & Bruyere, C. L. (2015). Changes in large-scale controls of Atlantic tropical cyclone activity with the phases of the Atlantic multidecadal oscillation. *Climate Dynamics*, *44*(7-8), 1801–1821. https://doi.org/10.1007/s00382-014-2186-5

Cole, J. E., & Cook, E. R. (1998). The changing relationship between ENSO variability and moisture balance in the continental United States. *Geophysical Research Letters*, *25*(24), 4529–4532. https://doi.org/10.1029/1998GL900145

Cook, E. R., & Kairiukstis, L. (1990). *Methods of Dendrochronology*. New York: Springer. https://doi.org/10.1007/978-94-015-7879-0

Cook, E. R., Meko, D. M., Stahle, D. W., & Cleaveland, M. K. (1999). Drought reconstructions of the continental United States. *Journal of Climate*, *12*(4), 1145–1162. https://doi.org/10.1175/1520-0442(1999)012<1145:DRFTCU>2.0.CO;2

Cook, E. R., Seager, R., Heim, R. R. Jr., Vose, R. S., Herweijer, C., & Woodhouse, C. (2010). Megadroughts in North America: Placing IPCC projections of hydroclimatic change in a long-term paleoclimate context. *Journal of Quaternary Science*, *25*(1), 48–61. https://doi.org/10.1002/jqs.1303

D'Arrigo, R., Cook, E. R., Wilson, R. J., Allan, R., & Mann, M. E. (2005). On the variability of ENSO over the past six centuries. *Geophysical Research Letters*, *32*, L03711. https://doi.org/10.1029/2004GL022055

d'Orgeville, M., & Peltier, W. R. (2007). On the Pacific Decadal Oscillation and the Atlantic Multidecadal Oscillation: Might they be related? *Geophysical Research Letters*, *34*, L23705. https://doi.org/10.1029/2007GL031584

Dai, A., & Wigley, T. M. L. (2000). Global patterns of ENSO-induced precipitation. *Geophysical Research Letters*, *27*(9), 1283–1286. https://doi.org/10.1029/1999GL011140

Douglas, A.V. (2007). Summer precipitation variability over Mexico. AGU Joint Assembly, Acapulco, Mexico. May 2007.

Enfield, D. B., Mestas-Nuñez, A. M., & Trimble, P. J. (2001). The Atlantic multidecadal oscillation and its relation to rainfall and river flows in the continental U.S. *Geophysical Research Letters*, *28*(10), 2077–2080. https://doi.org/10.1029/2000GL012745

Gergis, J. L., & Fowler, A. M. (2006). How unusual was late 20th century El Niño-Southern Oscillation (ENSO)? Assessing evidence from tree-ring, coral, ice-core and documentary palaeoarchives, A.D. 1525-2002. *Advances in Geosciences*, *6*, 173–179. https://doi.org/10.5194/adgeo-6-173-2006

Gergis, J. L., & Fowler, A. M. (2009). A history of ENSO events since A.D. 1525: implications for future climate change. *Climate Change*, *92*(3-4), 343–387. https://doi.org/10.1007/s10584-008-9476-z

Gray, S. T., Graumlich, L. J., Betancourt, J. L., & Pederson, G. T. (2004). A tree-ring based reconstruction of the Atlantic Multidecadal Oscillation since 1567 A.D. *Geophysical Research Letters*, *31*, L12205. https://doi.org/10.1029/2004GL019932

Grissino-Mayer, H. D., & Fritts, H. C. (1997). The International Tree-Ring Data Bank: An enhanced global database serving the global scientific community. *The Holocene*, *7*(2), 235–238. https://doi.org/10.1177/095968369700700212

Grudd, H., Briffa, K. R., Karlén, W., Batholin, T. S., Jones, P. D., & Kromer, B. (2002). A 7400-year tree-ring chronology in northern Swedish Lapland: Natural climatic variability expressed on annual to millennial timescales. *The Holocene*, *12*(6), 657–665. https://doi.org/10.1191/0959683602hl578rp

Harris, I., Jones, P. D., Osborn, T. J., & Lister, D. H. (2014). Updated high resolution grids of monthly climatic observation—The CRU TS3.10 dataset. *International Journal of Climatology*, *34*(3), 623–642. https://doi.org/10.1002/joc.3711

Herweijer, C., Seager, R., & Cook, E. R. (2006). North American droughts of the mid to late nineteenth century: A history, simulation and implication for Mediaeval drought. *The Holocene*, *16*(2), 159–171. https://doi.org/10.1191/0959683606hl917rp

Howard, I., Stahle, D. W., & Feng, S. (2019). Separate tree-ring reconstructions of spring and summer moisture in the northern and southern Great Plains. *Climate Dynamics*, *52*(9-10), 5877–5897. https://doi.org/10.1007/s00382-018-4485-8

Jauregui, E. (1979). Algunos aspectos de las fluctuaciones pluviometricas en Mexico en los ultimos cien anos. *Boletin del Instituto Geográfica UNAM*, *9*, 39–63.

Jolliffe, I. T. (2002). *Principal Component Analysis*. New York: Springer.

Kitzberger, T., Brown, P. M., Heyerdahl, E. K., Swetnam, T. W., & Veblen, T. T. (2007). Contingent Pacific-Atlantic Ocean influence on multicentury wildfire synchrony over western North America. *Proceedings of the National Academy of Sciences of the United States of America*, *104*(2), 543–548. https://doi.org/10.1073/pnas.0606078104

Li, J., Xie, S. P., Cook, E. R., Morales, M. S., Christie, D. A., Johnson, N. C., et al. (2013). El Niño modulations over the past seven centuries. *Nature Climate Change*, *3*(9), 822–826. https://doi.org/10.1038/nclimate1936

Lloyd, C. (2010). *Spatial Data Analysis*. Oxford, UK: Oxford University Press.

Lough, J.M., & Fritts, H.C. (1990). Historical aspects of El Niño/Southern Oscillation—Information from tree rings. *Elsevier Oceanography Series 52*: 285-321. https://doi.org/10.1016/S0422-9894(08)70039-4

Mann, M. E., Bradley, R. S., & Hughes, M. K. (2000). Long-term variability in the El Niño Southern Oscillation and associated teleconnections. In H. F. Diaz & V. Markgraf (Eds.), *El Niño and the Southern Oscillation: Multi-scale Variability and Its Impacts on Natural Ecosystems and Society* (Chap. 10, pp. 357–410). Cambridge, UK: Cambridge University Press.

Mantua, N. J., Hare, S. R., Zhang, Y., Wallace, J. M., & Francis, R. C. (1997). A Pacific interdecadal climate oscillation with impacts on salmon production. *Bulletin of the American Meteorological Society*, *78*(6), 1069–1079. https://doi.org/10.1175/1520-0477(1977)078<1069:APICOW>2.0.CO;2

McCabe, G. J., Palecki, M. A., & Betancourt, J. L. (2004). Pacific and Atlantic Ocean influences on multidecadal drought frequency in the United States. *Proceedings of the National Academy of Sciences of the United States of America*, *101*(12), 4136–4141. https://doi.org/10.1073/pnas.0306738101

Palmer, W. C. (1965). *Meteorological drought*, *Weather Bureau Research Paper*, (Vol. 45). Washington, DC: U.S. Department of Commerce.

Percival, D. B., & Constantine, W. L. B. (2006). Exact simulation of Gaussian time series from nonparametric spectral estimates with application to bootstrapping. *Statistics and Computing*, *16*(1), 25–35. https://doi.org/10.1007/s11222-006-5198-0

Ruprich-Robert, Y. (2018). Impacts of the Atlantic Multidecadal Variability on North American summer climate and heat waves. *Journal of Climate*, *31*(9), 3679–3700. https://doi.org/10.1175/JCLI-D-17-0270.1

Stahle, D. W., Burnette, D. J., Diaz, J. V., Heim, R. R., Fye, F. K., Paredes, J. C., et al. (2011). Pacific and Atlantic influences on Mesoamerican climate over the past millennium. *Climate Dynamics*, *39*(6), 1431–1446. https://doi.org/10.1007/s00382-011-1205-z

Stahle, D. W., & Cleaveland, M. K. (1988). Texas drought history reconstructed and analyzed from 1698 to 1980. *Journal of Climate*, *1*(1), 59–74. https://doi.org/10.1175/1520-0442(1988)001<0059:TDHRAA>2.0.CO;2

Stahle, D. W., & Cleaveland, M. K. (1993). Southern Oscillation extremes reconstructed from tree-rings of the Sierra Madre Occidental and the southern Great Plains. *Journal of Climate*, *6*(1), 129–140. https://doi.org/10.1175/1520-0442(1993)006<0129:SOERFT>2.0.CO;2

Stahle, D. W., Cook, E. R., Burnette, D. J., Villanueva, J., Cerano, J., Burns, J. N., et al. (2016). The Mexican Drought Atlas: Tree-ring reconstructions of the soil moisture balance during the late pre-Hispanic, Colonial, and modern Eras. *Quaternary Science Reviews*, *149*, 34–60. https://doi.org/10.1016/j.quascirev.2016.06.018

Stahle, D. W., Cleaveland, M. K., Therrell, M. D., Gay, D. A., D'Arrigo, R. D., Krusic, P. J., et al. (1998). Experimental dendroclimatic reconstruction of the Southern Oscillation. *Bulletin of the American Meteorological Society*, *79*(10), 2137–2152. https://doi.org/10.1175/1520-0477(1998)079<2137:EDROTS>2.0.CO;2

Sutton, R. T., & Hodson, L. R. (2005). Atlantic forcing of North American and European summer climate. *Science*, *309*(5731), 115–118. https://doi.org/10.1126/science.1109496

Torbenson, M. C. A., & Stahle, D. W. (2018). The relationship between cool and warm season moisture over the central United States, 1685-2015. *Journal of Climate*, *31*(19), 7909–7924. https://doi.org/10.1175/JCLI-D-17-0593.1

Torbenson, M. C. A., Stahle, D. W., Villanueva Díaz, J., Cook, E. R., & Griffin, D. (2016). The relationship between earlywood and latewood ring-growth across North America. *Tree-Ring Research*, *72*(2), 53–66. https://doi.org/10.3959/1536-1098-72.02.53

van Oldenborgh, G. J., & Burgers, G. (2005). Searching for decadal variations in ENSO precipitation teleconnections. *Geophysical Research Letters*, *32*, L023110. https://doi.org/10.1029/2005GL023110

Wahl, E. R., Diaz, H. F., Smerdon, J. E., & Ammann, C. M. (2014). Late winter temperature response to large tropical volcanic eruptions in temperate western North America: relationships to ENSO phases. *Global and Planetary Change*, *122*, 238–250. https://doi.org/10.1016/j.gloplacha.2014.08.005

Wilson, R., Cook, E., D'Arrigo, R., Riedwyl, N., Evans, M. N., Tudhope, A., & Allan, R. (2010). Reconstructing ENSO: The influence of method, proxy data, climate forcing and teleconnections. *Journal of Quaternary Science*, *25*(1), 62–78. https://doi.org/10.1002/jqs.1297

Wolter, K., & Timlin, M. S. (2011). El Niño/Southern Oscillation behaviour since 1871 as diagnosed in an extended multivariate ENSO index (MEI.ext). *International Journal of Climatology*, *31*(7), 1074–1087. https://doi.org/10.1002/joc.2336

Woodhouse, C. A., & Overpeck, J. T. (1998). 2000 years of drought variability in the central United States. *Bulletin of the American Meteorological Society*, *79*(12), 2693–2714. https://doi.org/10.1175/1520-0477(1998)079<2693:YODVIT>2.0.CO;2

Yocom, L. L., Fulé, P. Z., Brown, P. M., Cerano, J., Villanueva-Diaz, J., Falk, D. A., & Cornejo-Oviedo, E. (2010). El Niño-Southern Oscillation effect on a fire regime in northeastern Mexico has changed over time. *Ecology*, *91*(6), 1660–1671. https://doi.org/10.1890/09-0845.1

Yu, J.-Y., Kao, P.-K., Paek, H., Hsu, H.-H., Hung, C., Lu, M.-M., & An, S.-I. (2015). Linking emergence of the central Pacific El Niño to the Atlantic Multidecadal Oscillation. *Journal of Climate*, *28*(2), 651–662. https://doi.org/10.1175/JCLI-D-14-00347.1